Supporting Information

Ahmad et al. 10.1073/pnas.1109526109

SI Materials and Methods

α-Synuclein Mutants Production, Expression, and Purification. Four different tryptophan/cysteine (Trp/Cys) pair-containing α-synuclein mutants were created using the QuikChange Site-Directed Mutagenesis Kit (Stratagene) and DNA sequencing was used to ensure the presence of the desired mutations. The wild-type and mutant proteins were expressed in *Escherichia coli* BL21 (DE3) cells transformed with the T7-7 plasmid and purified as described previously (1). Briefly, after cell lysis, the cell suspension was boiled for 20 min and centrifuged at 13,000 rpm. The supernatant was collected and the protein was precipitated out by ammonium sulfate precipitation method. The pellet was resuspended in 25 mM Tris·HCl buffer (pH 7.4) and chromatographed on a Q-Sepharose Fast Flow column equilibrated with 25 mM Tris buffer (pH 7.4) and eluted with a linear NaCl gradient (0–1,000 mM). α-Synuclein-containing fractions were pooled and further purified by gel filtration on a Hi-Prep Sephacryl S200 column. α-Synuclein eluted as single peak and was found to be >95% pure as assessed by SDS-PAGE. The protein concentration was determined from the absorbance at 275 nm for wild-type and 280 nm for mutants using extinction coefficient of 5,600 M^{-1} cm^{-1} and 11,460 M^{-1} cm^{-1}, respectively. The stock solution of approximately 300 μM was stored at −80 °C in 25 mM sodium phosphate buffer (pH 7.4) with 1 mM tris(2-carboxyethyl)phosphine (TCEP). Shortly before the experiment, a 300 μL aliquot was thawed, filtered, and diluted 10:1 into cuvette containing sodium phosphate buffer (pH 7.4) or sodium acetate buffer (pH 3.5) and the final sucrose that had been thoroughly saturated with N_2O to scavenge solvated electrons and prevent O_2 quenching of the triplet.

Far-UV CD. Far-UV CD measurements were carried out with an AppliedPhotophysics Chirascan spectropolarimeter equipped with a thermostated cell holder. The spectra were acquired at the protein concentration of 6 μM, 0–40° C, in the absence and presence of 30% sucrose and using a 1 mm path-length cell. The spectra were recorded with 0.5–4 s adaptive integration time and 1 nm bandwidth. Each spectrum was the average of four scans. All the mutants and wild-type protein spectra are almost identical, and contain minima around 198 nm and absence of CD band in 210–230 nm, typical of unfolded polypeptide.

Thioflavine T (ThT) Fluorescence. Aggregation of each mutant was initiated by stirring the protein, at a concentration of 48 μM, in 25 mM phosphate buffer, pH 7.4, 150 mM NaCl, 1 mM TCEP, 37° C. At regular time interval aliquots of 60 μL of each mutant were mixed with 440 mL of 25 mM phosphate buffer, pH 7.4, containing 25 μM ThT and the resulting fluorescence was measured using a Jobin Yvon Spex Fluorolog-3 spectrofluorometer equipped with a thermostated cell holder. The excitation and emission wavelengths were 440 and 485 nm, respectively. A 10-mm path-length quartz cell was used.

FRET. FRET labeled protein was a kind gift from Elizabeth Rhoades, Yale University, New Haven, CT. The protein was mutated to have a cysteine at positions 9 and 70 and labeled with Alexa 488 and Alexa 594. The protein was diluted to 10 nM and measured using a PTI Technology QW4 spectrofluorimeter equipped with a thermostated cell holder. The excitation wavelength was 488 nm and emission was collected every 1 nm. FRET was calculated using the formula $E = I_A/(I_D + I_A)$, where I_D is the sum of intensities from 500 to 575 nm and I_A is the sum of intensities from 576 to 800 nm.

Extraction of Reaction-Limited and Diffusion-Limited Rates. Observed decay times ($1/k_{obs}$) at pH 7.4 are plotted versus η in Fig. S4. Examination of Fig. S4 shows that at each temperature, $1/k_{obs}$ versus η fits well to a line so each line is fit independently and the slopes and intercepts are plotted in Fig. 2. These plots are qualitatively different than any other disordered protein yet observed (see, for example, figure 6 in ref. 2 and figure 3 in ref. 3). Generally for other unstructured peptides or proteins in high denaturant, the intercept ($1/k_R$) and slope ($1/\eta k_{D+}$) both decrease gradually with temperature. Fig. 1*D* shows the intercept decreasing dramatically with temperature and the slope increasing with temperature. At the highest temperatures, the intercept is consistent with zero, implying that k_{obs} is diffusion-limited. For pH 3.5, fitting each temperature to a separate line yields zero intercepts for most temperatures for the 69W-94C and 112W-140C loops and some temperature for 4W-30C and 39W-69C (see Fig. S7). For all loops the slopes change very little with temperature. Therefore, for consistency, we fit all data for a single loop to a single line.

It is reasonable to assume (as has been done in previous studies) that the observed rates at pH 7.4 have an Arrhenius temperature dependence,

$$k_R = k_{R0} \exp\left[\frac{-E_1(T - T_0)}{RTT_0}\right] \quad \text{[S1]}$$

$$k_{D+} = \frac{k_{D+0}}{\eta} \exp\left[\frac{-E_2(T - T_0)}{RTT_0}\right]. \quad \text{[S2]}$$

Fig. S5 shows these fits for each loop at pH 7.4 and Table S1 gives the fitting parameters. For all loops $E_1 \sim 6$–8 kcal/mol and $E_2 \sim 4$ kcal/mol. In contrast, bimolecular quenching of Trp by Cys gives $E_1 \sim 2$ kcal/mol and $E_2 \sim 0$ (see Fig. S8) whereas for unstructured peptides and denatured proteins $E_1 \sim 4$ kcal/mol and $E_2 \sim -2$ kcal/mol. From these results we conclude that there is an activation energy for both q and $K = k_{D+}/k_{D-}$, which is significantly larger for α-synuclein than other sequences studied. Also, for unstructured peptides and denatured proteins the free energy of diffusion $E_2 = \Delta H - T\Delta S$ is dominated by entropy whereas for α-synuclein, E_2 is dominated by enthalpy. These conclusions indicate a picture of a chain that compacts with temperature and has strong intramolecular interactions that slow diffusion.

However, a close inspection of the Arrhenius fits show that they do not fit the data very well. Furthermore, pH 3.5, in which α-synuclein is more prone to aggregate than at neutral pH, measurements of $1/k_{obs}$ versus η at various temperatures all collapse to the same line (See Fig. S7). This behavior has been seen for the unfolded state of folded proteins in low denaturant and suggests that the chain is highly collapsed and diffusion is slow and temperature-independent. An Arrhenius model of these rates seems inconsistent unless the activation energies of both reaction-limited and diffusion-limited rates simultaneously go to zero at low pH. Instead, we can interpret these rates in the context of a glass transition. Whereas most glasses form as temperature is decreased, there are a few examples of glasses that exhibit inverse melting where the glass transition temperature is approached from below (4–8). A common formula to describe the temperature dependence of the viscosity before the glass transition is the Vogel–Fulcher–Tammann–Hesse (VFTH) equation (7). Because glass theory is usually applied to isotropic systems, there is no

prediction of how the reaction-limited rate should behave, therefore we use the same formalism as for k_{D+},

$$k_R = k_{R0}\exp\left(\frac{B_1}{T - T_{V1}}\right) \quad \textbf{[S3]}$$

$$k_{D+} = \frac{k_{D+0}}{\eta}\exp\left[\frac{B_2}{(T_{V2} - T)}\right]. \quad \textbf{[S4]}$$

Note that this form is quite similar to a sigmoid, which is a reasonable functional form for k_R if the chain undergoes a collapse transition. The fit parameters are given in Table S2 and a comparison of the sum of squares (*fss*) between the glass fits and the Arrhenius fits show that overall the glass fits are superior. Following this model, we can conclude that at pH 3.5, the chain is already glassy and therefore has no temperature dependence. However, in the absence of a realistic theory of polymer collapse, it is not clear the glass model is really the best one we can construct. Therefore, the subsequent analysis uses the simple fit of data at each temperature to a separate line. Note that all three fitting methods yield the same qualitative temperature dependence on k_R and k_{D+}.

Molecular Dynamics Simulations. Molecular dynamics simulations were performed using an accelerated version of GROMACS (9) written specifically for graphical processing units (GPUs) called OpenMM (10). The AMBERff99sb (11) force field was used with the generalized Born/surface area (GB/SA) implicit solvent model (12). The temperature was 273 K with water-like viscosity. Each simulation on each GPU started from a fully extended conformation and was followed for approximately 200 ns (1 wk of wall-clock time). Coordinates for each atom were saved every 200 ps. Each conformation was analyzed with the standard GROMACS package to determine intramolecular distances. A normalized histogram of all distances in all runs was created to be used in Eqs. **3** and **4**.

Energy-Reweighted Worm-Like Chain (WLC) Modeling and Determination of Effective Diffusion Coefficient. All the mutants studied experimentally were modeled with energy-reweighted WLC model (13). Briefly, for each WLC conformation of a particular mutant, a total energy (E_{TOT}) is defined, that is the sum of pairwise interactions between the C^α atoms,

$$E_{\mathrm{TOT}} = -\sum_{i-j>1}\frac{e_{i,j}}{|r_i - r_j|} \quad \textbf{[S5]}$$

$$e_{i,j} = \begin{cases} 0, & |h_i - h_j| > 0.3 \\ \sigma, & |h_i - h_j| \le 0.3 \end{cases},$$

where, i and j are the indices of two nonadjacent residues, $|r_i - r_j|$ is the distance between these two residues, which must be larger than d_α and less than 6.5 Å, and h_i and h_j are the normalized hydrophobicities of the two residues as determined by the Miyazawa Jernigan scale. The strength of the hydrophobic potential between two residues, $e_{i,j}$, equals zero if one is hydrophobic and one is hydrophilic and equals an adjustable parameter, σ, if both are hydrophobic or hydrophilic. The parameter, σ, (in units of $kT \cdot$ Å) exhibits the strength of the hydrophobic interaction and is tunable according to various solvent conditions.

Using E_{TOT} and r as independent reaction coordinates, a two-dimensional probability distribution $P(r,E_{\mathrm{TOT}})$ is defined so that,

$$1 = \int dr \int dE_{\mathrm{TOT}} P(r,E_{\mathrm{TOT}}) \quad \textbf{[S6]}$$

and the one-dimensional Trp-Cys distance distribution is defined as $P(r) = \int P(r,E_{\mathrm{TOT}})dE_{\mathrm{TOT}}$. Let $Z(r)$ represent the energy-reweighted distribution of distance r between the Trp and Cys C^α position. $Z(r)$ can be written as follows:

$$\begin{aligned} Z(r) &= N \cdot \int P(r,E_{\mathrm{TOT}})\exp(-E_{\mathrm{TOT}}/kT)dE_{\mathrm{TOT}} \\ &= N \cdot \int P(r,E_{\mathrm{TOT}})dE_{\mathrm{TOT}} \cdot \frac{\int P(r,E_{\mathrm{TOT}})\exp(-E_{\mathrm{TOT}}/kT)dE_{\mathrm{TOT}}}{\int P(r,E_{\mathrm{TOT}})dE_{\mathrm{TOT}}} \\ &= N \cdot P(r) \cdot \langle \exp(-E_{\mathrm{TOT}}/kT)\rangle_r \\ \frac{1}{N} &= \int_{d_\alpha}^{l_c} P(r) \cdot \langle \exp(-E_{\mathrm{TOT}}/kT)\rangle_r dr. \end{aligned} \quad \textbf{[S7]}$$

Using Eq. **S7** and Eq. **3**, we have found $Z(r)$ for each mutant in each condition that best matches the experimental reaction-limited rate. Table S3 gives the values of σ for each loop and solvent condition. Then the appropriate $Z(r)$ and experimental k_{D+} is used in Eq. **4** to determine the effective diffusion coefficients. To determine the average radius of gyration (R_G) used in determining the reconfiguration time (τ), R_G for each chain was determined and a $P(R_G)$ created and reweighted using the E_{TOT} determined from the Trp-Cys distance for a given σ.

1. Eliezer D, Kutluay E, Bussell R, Browne G (2001) Conformational properties of α-synuclein in its free and lipid-associated states. *J Mol Biol* 307:1061–1073.
2. Singh VR, Kopka M, Chen Y, Wedemeyer WJ, Lapidus LJ (2007) Dynamic similarity of the unfolded states of proteins L and G. *Biochemistry* 46:10046–10054.
3. Chen YJ, Parrini C, Taddei N, Lapidus LJ (2009) Conformational properties of unfolded HypF-N. *J Phys Chem B* 113:16209–16213.
4. Angelini R, Ruocco G (2007) Viscosity measurements in a solution undergoing inverse melting. *Philos Mag* 87:553–558.
5. Angelini R, Ruocco G, De Panfilis S (2008) Phase diagram of a solution undergoing inverse melting. *Phys Rev E* 78:020502.
6. Rastogi S, Höhne GWH, Keller A (1999) Unusual pressure-induced phase behavior in crystalline poly(4-methylpentene-1): Calorimetric and spectroscopic results and further implications. *Macromolecules* 32:8897–8909.
7. Roland CM (2010) Relaxation phenomena in vitrifying polymers and molecular liquids. *Macromolecules* 43:7875–7890.
8. Schupper N, Shnerb NM (2004) Spin model for inverse melting and inverse glass transition. *Phys Rev Lett* 93:037202.
9. Van der Spoel D, et al. (2005) GROMACS: Fast, flexible, and free. *J Comput Chem* 26:1701–1718.
10. Friedrichs MS, et al. (2009) Accelerating molecular dynamic simulation on graphics processing units. *J Comput Chem* 30:864–872.
11. Hornak V, et al. (2006) Comparison of multiple amber force fields and development of improved protein backbone parameters. *Proteins* 65:712–725.
12. Onufriev A, Bashford D, Case DA (2004) Exploring protein native states and large-scale conformational changes with a modified generalized born model. *Proteins* 55:383–394.
13. Chen Y, Wedemeyer WJ, Lapidus LJ (2010) A general polymer model of unfolded proteins under folding conditions. *J Phys Chem B* 114:15969–15975.

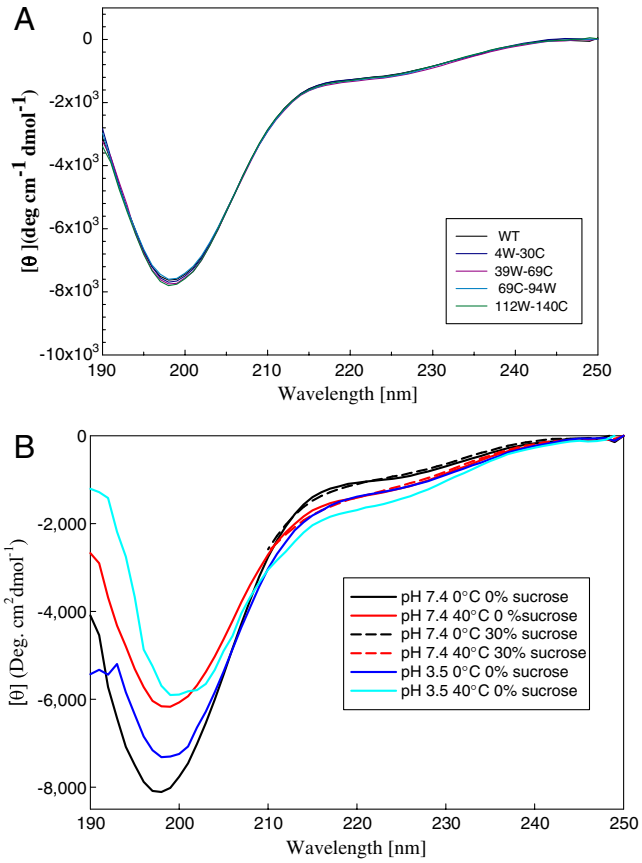

Fig. S1. (*A*) Comparison of far-UV CD spectra of the four α-synuclein mutants with wild-type protein at pH 7.4, 37° C. (*B*) Far-UV CD spectra of 39W-69C mutant in the absence and presence of 30% sucrose (vol/vol) at 0 and 40° C at pH 7.4 and pH 3.5, respectively.

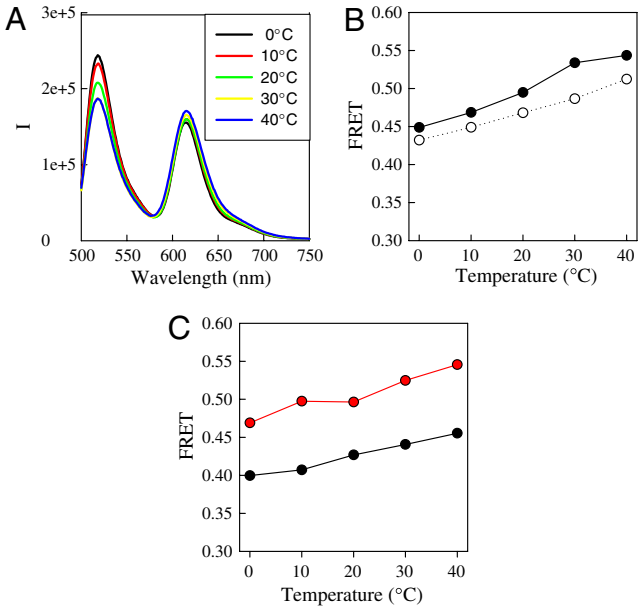

Fig. S2. (*A*) Fluorescent spectra of FRET labeled α-synuclein at various temperatures. (*B*) FRET values at various temperatures with (white points) and without (black points) 30% sucrose at pH 7.4. (*C*) FRET values at various temperatures at pH 7.4 (black points) and pH 3.5 (red points). Measurements in *B* and *C* were made in different samples with different fluorescence labeling efficiencies.

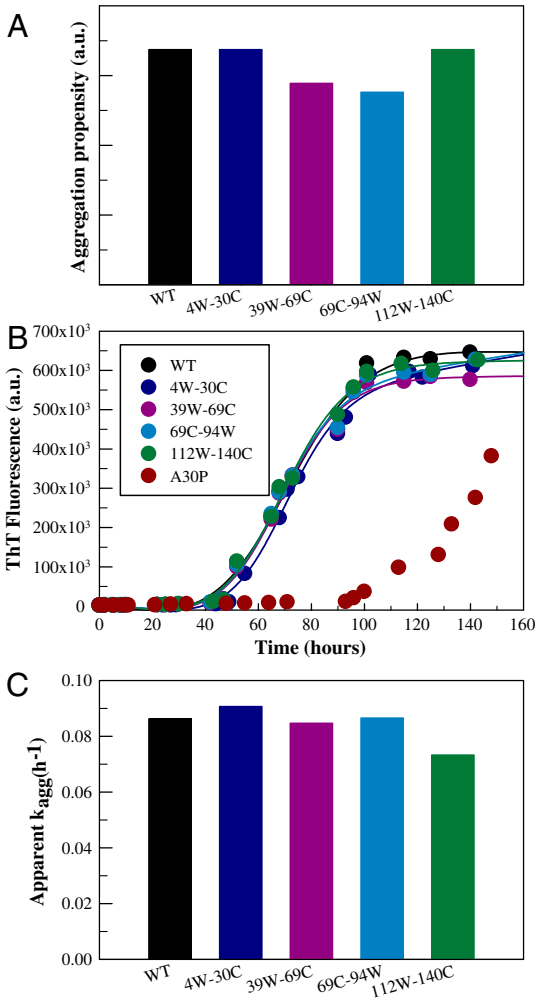

Fig. S3. (*A*) Intrinsic aggregation propensity of Trp-Cys α-synuclein mutants and wild-type calculated using the Tango algorithm. (*B*) Time courses of ThT fluorescence for wild-type and all the α-synuclein mutants. All of the mutants and wild-type proteins are consistent with the nucleation-dependent polymerization model, which comprises a nucleation phase, an exponential growth phase, and a final equilibrium phase. The ThT traces were satisfactorily fitted to a sigmoidal function as described by the following equation,

$$F = F_0 + m_0 x + \frac{F_1 + m_1 x}{1 + e^{-[(x - x_{1/2})/\tau]}},$$

where F_0 is the observed ThT fluorescence intensity, x is time, and $x_{1/2}$ is the time to 50% of maximum fluorescence. Therefore, the apparent rate constant, k_{app}, for the aggregation is given by $1/\tau$, shown in *C*, and the lag time is given by $x_{1/2} - 2\tau$.

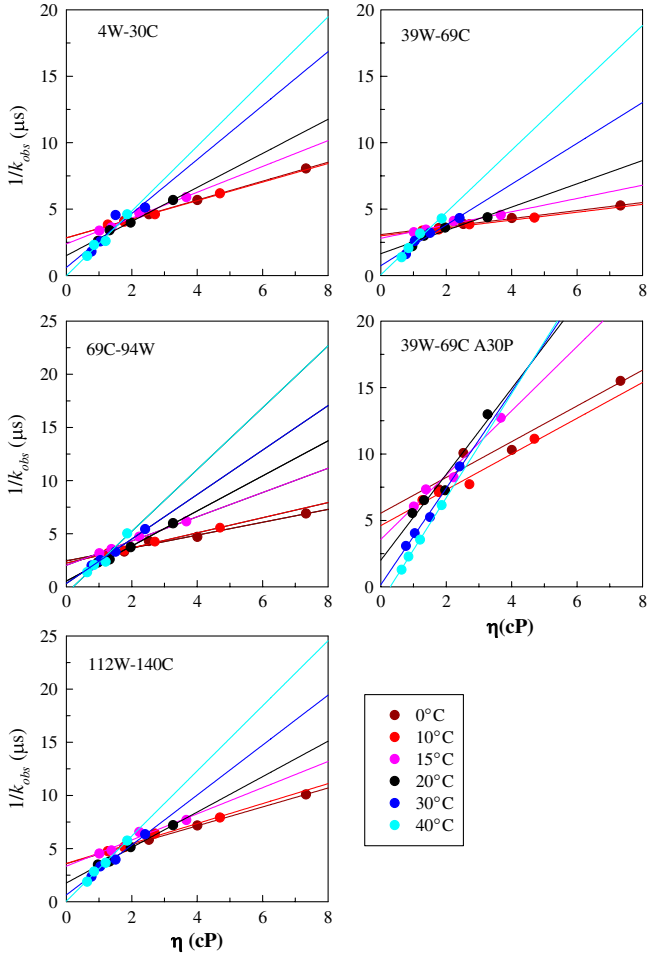

Fig. S4. Viscosity (η) versus $1/k_{obs}$ at pH 7.4 for the various loops as marked. The data at each temperature is fit to a separate line. The intercept and slope of each fit determines k_R and k_{D+} plotted in Fig. 2 *A* and *C*. The k_{D+} are calculated for the viscosity of water at each temperature.

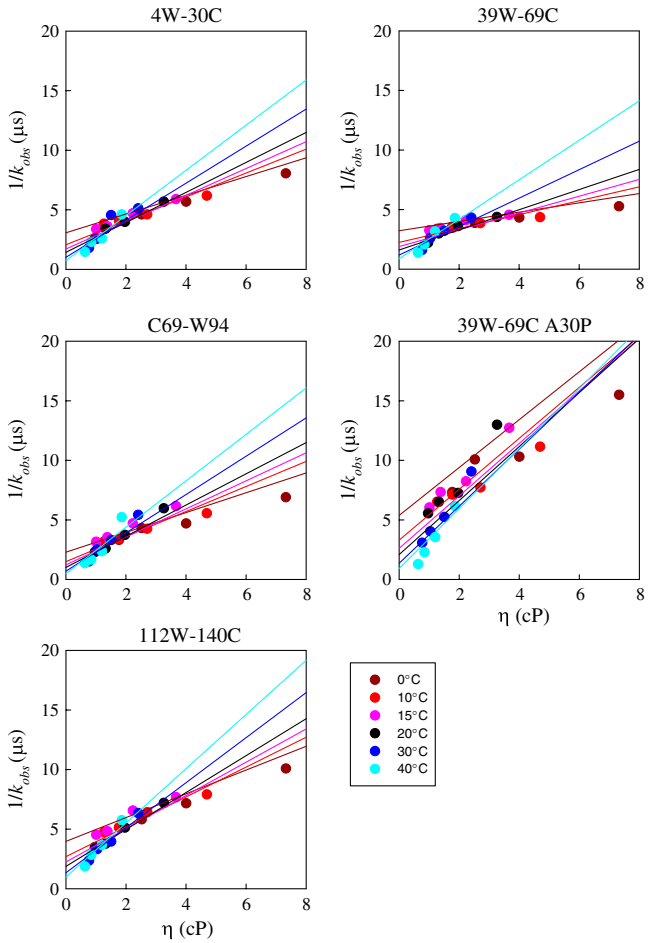

Fig. S5. Viscosity (η) versus $1/k_{obs}$ at pH 7.4 for the various loops as marked. The data on each plot is globally fit to an Arrhenius model Eqs. **S1** and **S2**.

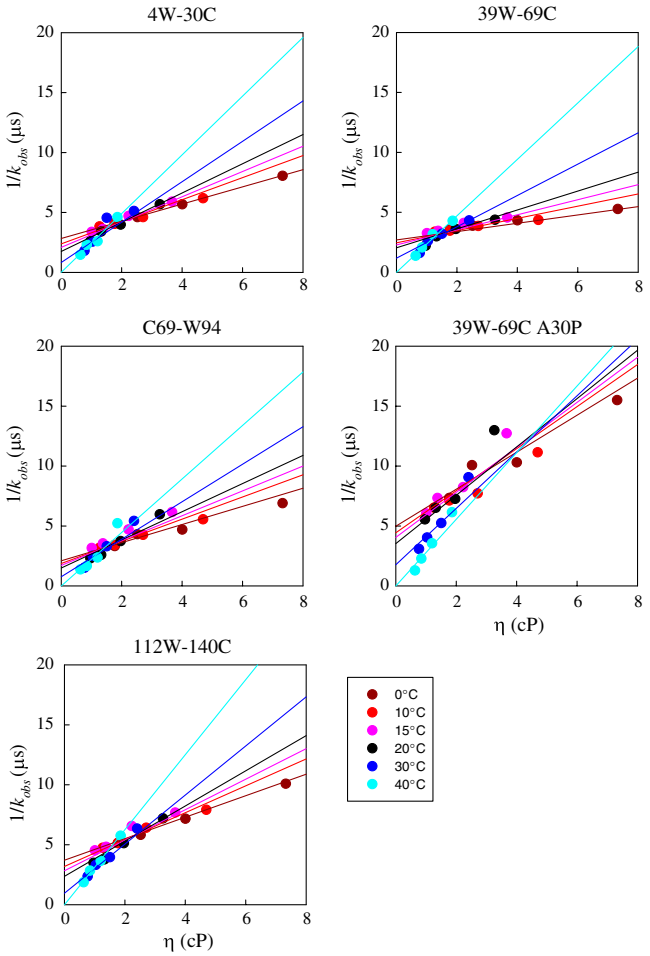

Fig. S6. Viscosity (η) versus $1/k_{obs}$ at pH 7.4 for the various loops as marked. The data on each plot is globally fit to a glass transition model Eqs. **S3** and **S4**.

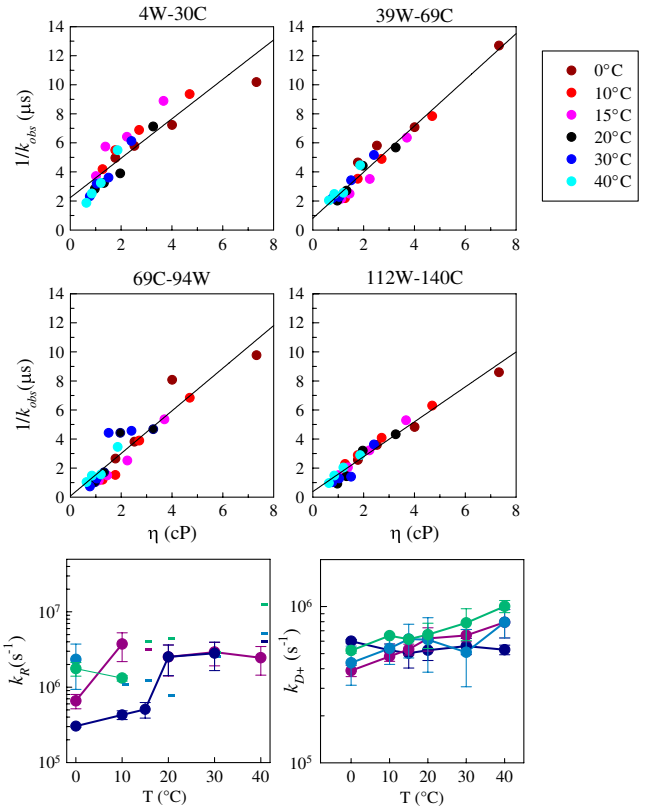

Fig. S7. Viscosity (η) versus $1/k_{obs}$ at pH 3.5 for the various loops as marked. Lines are fits of all data at all temperatures. The intercept and slope of each fit determines k_R and k_{D+} (at $\eta = 1$ cP) plotted in Fig. 2 *B* and *D*. (*Bottom*) The k_R and k_{D+} (at the viscosity of water at each temperature) when each temperature is fit to a separate line using the color code in the main text. The dashes show the lower limit of k_R determined from the error in the intercept.

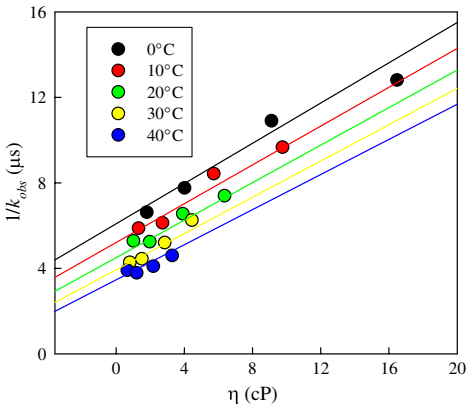

Fig. S8. Viscosity (η) versus $1/k_{obs}$ of 100 μM *N*-actyl tryptophan amide and 500 μM cysteine. The data is fit globally to Eqs. **S1** and **S2**.

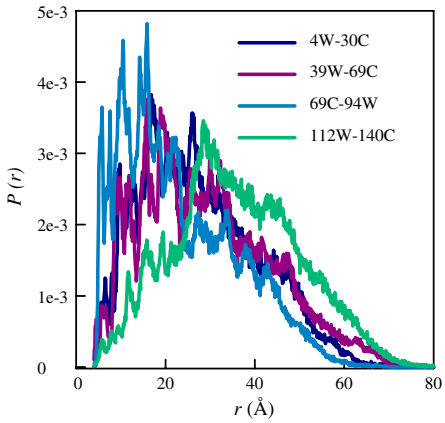

Fig. S9. Probability distributions of Trp-Cys distances calculated from molecular dynamics simulations. Reaction-limited rates calculated from these distributions are shown in Fig. 2*B*.

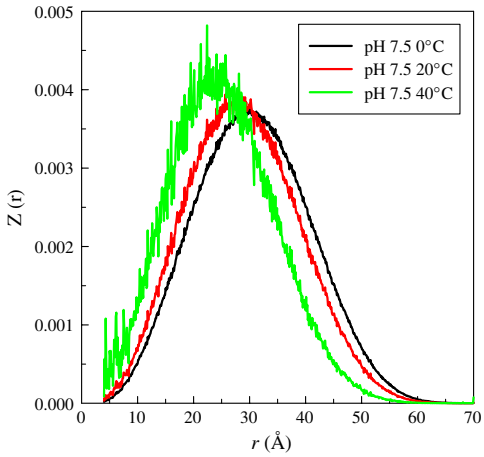

Fig. S10. Probability distributions [$Z(r)$] of 69C-94W distance calculated by the energy-reweighted WLC model. The lines are the distributions that best predict k_R at each of the solution conditions on the legend.

Table S1. Fit parameters for Arrhenius fits of measurements at pH 7.4

Sequence	k_{R0} (s^{-1})	E_1 (kcal/mol)	k_{D+0}(s^{-1})	E_2 (kcal/mol)	*fss**
4W-30C	7.0×10^5	6.1	7.9×10^5	3.7	0.0696
39W-69C	6.2×10^5	5.5	1.2×10^5	6.1	0.0844
39W-69C A30P	4.8×10^5	7.5	4.4×10^5	0.96	0.2365
69C-94W	1.0×10^6	6.5	7.6×10^5	3.6	0.1166
112W-140C	5.3×10^5	5.9	6.5×10^5	3.5	0.0563

*Sum of squared difference between fit and measured values, in log space, $fss = \sum[\log(k_{\text{fit}}) - \log(k_{\text{measured}})]^2$.

Table S2. Fit parameters for glass fits of measurements at pH 7.4

Sequence	k_{R0} (s^{-1})	B_1 (K)	T_{V1} (K)	k_{D+0} (s^{-1})	B_2 (K)	T_{V2} (K)	*fss**
4W-30C	2.0×10^5	26.1	317	6.4×10^7	633	438	0.0359
39W-69C	2.8×10^5	11.3	313	9.4×10^8	931	434	0.0460
39W-69C A30P	1.4×10^5	13.8	313	1.2×10^7	701	512	0.0709
69C-94W	3.4×10^5	13.4	313	1.3×10^7	287	398	0.0688
112W-140C	1.7×10^5	18.0	313	1.1×10^7	263	387	0.0172

*Sum of squared difference between fit and measured values, in log space, $fss = \sum[\log(k_{\text{fit}}) - \log(k_{\text{measured}})]^2$.

Table S3. Values of σ used to fit measured k_R

	pH 7.4						pH 3.5
Sequence	0° C	10° C	15° C	20° C	30° C	40° C	
4W-30C	0.9	0.9	1.2	1.6	2.8	3.0	1.2
39W-69C	0.5	0.5	0.78	1.2	2.5	2.5	1.65
39W-69C A30P	0.4	0.5	0.65	1.05	2.7	3.0	—
69C-94W	0.9	1.0	1.1	2.3	3.0	3.0	3.0
112W-140C	0.0	0.0	0.0	0.6	1.9	3.0	2.5